

Exact solution of slow quench dynamics and nonadiabatic characterization of topological phases

Rui Wu(邬睿), Panpan Fang(房盼攀), Chen Sun(孙辰), and Fuxiang Li(李福祥)

Citation: Chin. Phys. B, 2023, 32 (**8**): 080304. DOI: 10.1088/1674-1056/acd0a5
Journal homepage: http://cpb.iphy.ac.cn; http://iopscience.iop.org/cpb

What follows is a list of articles you may be interested in

High-fidelity topological quantum state transfers in a cavity-magnon system

Xi-Xi Bao(包茜茜), Gang-Feng Guo(郭刚峰), Xu Yang(杨煦), and Lei Tan(谭磊)
Chin. Phys. B, 2023, 32 (**8**): 080301. DOI: 10.1088/1674-1056/acc3f6

Nonadiabatic geometric phase in a doubly driven two-level system

Weixin Liu(刘伟新), Tao Wang(汪涛), and Weidong Li(李卫东)
Chin. Phys. B, 2023, 32 (**5**): 050311. DOI: 10.1088/1674-1056/ac89e3

Collapses-revivals phenomena induced by weak magnetic flux in diamond chain

Na-Na Chang(常娜娜), Wen-Quan Jing(景文泉), Yu Zhang(张钰), Ai-Xia Zhang(张爱霞), Ju-Kui Xue(薛具奎), Su-Peng Kou(寇谡鹏)
Chin. Phys. B, 2020, 29 (**1**): 010306. DOI: 10.1088/1674-1056/ab6087

The upper bound function of nonadiabatic dynamics in parametric driving quantum systems

Lin Zhang(张林), Junpeng Liu(刘军鹏)
Chin. Phys. B, 2019, 28 (**8**): 080301. DOI: 10.1088/1674-1056/28/8/080301

Accelerating an adiabatic process by nonlinear sweeping

Cao Xing-Xin (曹兴鑫), Zhuang Jun (庄军), Ning Xi-Jing (宁西京), Zhang Wen-Xian (张文献)
Chin. Phys. B, 2013, 22 (**9**): 090310. DOI: 10.1088/1674-1056/22/9/090310

Exact solution of slow quench dynamics and nonadiabatic characterization of topological phases

Rui Wu(邬睿), Panpan Fang(房盼攀), Chen Sun(孙辰), and Fuxiang Li(李福祥)†

School of Physics and Electronics, Hunan University, Changsha 410082, *China*

(Received 7 January 2023; revised manuscript received 23 April 2023; accepted manuscript online 27 April 2023)

Previous studies have shown that the bulk topology of single-particle systems can be captured by the band inversion surface or by the spin inversion surface emerging on the time-averaged spin polarization. Most of the studies, however, are based on the single-particle picture even though the systems are fermionic and multi-bands. Here, we study the slow quench dynamics of topological systems with all the valence bands fully occupied, and show that the concepts of band inversion surface and spin inversion surface are still valid. More importantly, the many-particle nonadiabatic quench dynamics is shown to be reduced to a new and nontrivial three-level Landau–Zener model. This nontrivial three-level Landau–Zener problem is then solved analytically by applying the integrability condition and symmetry considerations, and thus adds a new member to the few models that are exactly solvable. Based on the analytical results, the topological spin texture revealed by the time-averaged spin polarization can be applied to characterize the bulk topology and thus provides a direct comparison for future experiments.

Keywords: Landau–Zener, slow quench, nonadiabatic

PACS: 03.65.Vf, 33.50.Hv, 71.70.Di **DOI:** 10.1088/1674-1056/acd0a5

1. Introduction

Since the discovery of the integer quantum Hall effect in the 1980s,[1] the concept of topological insulator has ignited extensive interests in condensed matter physics.[2–4] Although this concept was first proposed in the electronic systems, it has been extended to almost all branches of physics from optics, acoustics, and mechanics to magnetics and spintronics.[5–7] The most exotic property of topological insulators is that they can support protected boundary states that are immune to moderate disorder or defects.[8] In addition, according to the bulk-boundary correspondence, the number of these boundary states is related to the bulk topological invariant of the topological phases.[9,10] Thus, how to characterize bulk topology of the systems plays an important role in exploring the properties of topological insulator.

However, in the context of traditional band topology, most of previous studies about topological characterization focus on the thermodynamically equilibrium systems, while the topological characterization of far from equilibrium systems is less known in general. In the last two decades, due to the rapid development of technology in quantum manipulation and measurement of ultracold atoms,[11–13] the platforms of well-designed optical lattice have emerged in quantum physics, where the systems can undergo a dynamical topological transition by dynamically tuning the Hamiltonian parameters, or coupling the systems to a nonequilibrium bath.[14–16] Due to its unique advantages in characterizing the topological properties of systems, there have emerged lots of detection methods of nonequilibrium, such as dynamical quantum phase transition (DQPT),[17–20] entanglement spectrum (ES),[21,22] and dynamical winding number (DWN),[23] etc. Notably, Liu and his co-workers proposed a new dynamical characterization theory based on quantum quench dynamics which has been verified experimentally in Hermitian systems.[24–29] They established a dynamical bulk-surface correspondence, which states a generic dD topological phase with $\mathbb{Z}$-type invariants can be characterized by the $(d-1)$D invariants defined on the so-called band inversion surface (BIS). Based on the higher-order BIS, they then extended their characterization scheme to other AZ tenfold classes of topological phases including $\mathbb{Z}_2$-type invariants. By suddenly quenching the system from a trivial phase to a topological phase, the bulk topology of the dD equilibrium phases of the post-quench Hamiltonian can be easily determined by the BIS emerged on the time-averaged spin polarization (TASP).

Nevertheless, most of the previous studies are based on the single-particle picture even though the systems are fermionic and of multi-bands. Nonequilibrium quantum many-body systems may exhibit novel phenomena that are completely different from the traditional equilibrium many-body systems.[30,31] Thus, many fundamental concepts, such as the spontaneous symmetry breaking and the topological order, need to be reexamined in the background of nonequilibrium physics. In the case of dynamical characterization, it would be necessary to investigate the effect of the Pauli exclusion principle and interaction effect when the energy levels are occupied by more than one particle.

In this paper, rather than characterizing the single-particle

†Corresponding author. E-mail: fuxiangli@hnu.edu.cn

© 2023 Chinese Physical Society and IOP Publishing Ltd

systems, we ask how the dynamical topological characterization should be performed in many-particle fermionic systems by considering the Pauli exclusion principle. Specifically, we study the four-band topological systems with two lower bands (valence bands) being fully occupied. We show that, in such systems, the dynamics is controlled by an effective 3×3 Hamiltonian. Therefore, when considering the slow quench dynamics starting from the deep trivial phases to the topological phases,[32,33] one encounters a nontrivial three-state Landau–Zener (LZ) problem. By investigating the intrinsic symmetry of scattering matrix and utilizing the integrability conditions,[34–37] we solve this new LZ model, thus adding a new ingredient into the class of exactly solvable time-dependent models. The time averaged spin polarization can then be obtained analytically as a function of quenching rate. We further obtain the topological spin texture on the position of BIS and spin inversion surface (SIS), and thus the dynamical characterization of bulk topology can be construed.

The rest of the paper is organized as follows. In Section 2, we introduce a 4×4 Hamiltonian for the single-particle system, and then extend it to a 6×6 Hamiltonian in the case with the valence bands being fully occupied. In Section 3, we consider the sudden quench dynamics and slow nonadiabatic quench dynamics of these systems, respectively. In Section 4, we analytically solve the three-level Landau–Zener problem. In Section 4, we apply the model Hamiltonian to the $\mathbb{Z}_2$-type and $\mathbb{Z}$-type topological insulator and present the dynamical characterization under slow nonadiabatic quench dynamics. A brief discussion of the case with symmetry-breaking term and interaction effect is presented in Section 4. Finally, a conclusion is given in Section 5.

2. Hamiltonian of the topological system

We first present the theoretical framework of the many-particle version of a four-band topological system with the two valence bands being fully occupied. Specifically, we consider a large class of topological phases whose matrix representations are 4×4. The corresponding single-particle Hamiltonian is usually expressed in terms of Gamma matrices

$$\boldsymbol{H}_{\rm s}(\boldsymbol{k})=\boldsymbol{h}(\boldsymbol{k})\cdot\boldsymbol{\gamma}=\sum_{j=0}^{d}h_j(\boldsymbol{k})\gamma_j, \tag{1}$$

where $\boldsymbol{h}(\boldsymbol{k})$ is an effective field which depends on the Bloch momentum $\boldsymbol{k}$ in Brillouin zone. $\boldsymbol{\gamma}_j$ are 4×4 matrices and obey the Clifford algebra $\{\gamma_j,\gamma_l\}=2\delta_{jl}$ for $j,l=0,1,\ldots,d$. This Hamiltonian can describe the 3D $\mathbb{Z}$-type insulators and $\mathbb{Z}_2$ topological insulators, corresponding to $d=3$ and $d=4$, respectively. Without loss of generality, we choose the following convention for Gamma matrices: $\gamma_0=\sigma_z\otimes\sigma_0$, $\gamma_1=\sigma_x\otimes\sigma_z$, $\gamma_2=\sigma_y\otimes\sigma_0$, $\gamma_3=\sigma_x\otimes\sigma_x$, $\gamma_4=\sigma_x\otimes\sigma_y$, with $\sigma_{x,y,z}$ being the three Pauli matrices and σ_0 being the 2×2 identity matrix. In matrix form, the single-particle Hamiltonian $\boldsymbol{H}_{\rm s}$ can be written explicitly as

$$\boldsymbol{H}_{\rm s}=\begin{pmatrix}h_0 & 0 & h_- & h'_-\\ 0 & h_0 & h'_+ & -h_+\\ h_+ & h'_- & -h_0 & 0\\ h'_+ & -h_- & 0 & -h_0\end{pmatrix}, \tag{2}$$

where, for simplicity, we introduce two new parameters $h_\pm=h_1\pm\mathrm{i}h_2$ and $h'_\pm=h_3\pm\mathrm{i}h_4$. The eigenvalues of the $\boldsymbol{H}_{\rm s}$ are

$$E_\pm=\pm\varepsilon,\ \text{ with }\ \varepsilon=\sqrt{\sum_{j=0}^{4}h_j^2}.$$

Both of the two eigenvalues are doubly degenerate as shown in Fig. 1(a).

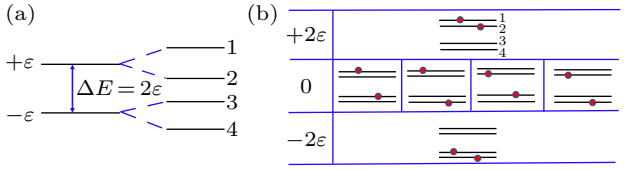


Fig. 1. (a) The graphic diagram of the energy levels of the single-particle systems. Here, both the upper and lower bands are doubly degenerate. We denote the sub-band as $1,2,3,4$ from top to bottom, respectively. (b) The electron occupation on each energy level in the many-particle system. The red balls and the black lines represent the electrons and the energy levels, respectively.

In the nonequilibrium quench dynamics of the topological phases, most of the previous studies only consider the single-particle state.[24,32,38,39] However, in the real experiments, what one should prepare is actually a many-particle state with the two degenerate valence bands fully occupied.[25–27] Thus, it is necessary to consider a many-particle version of the Hamiltonian with two non-interacting fermions for each momentum $\boldsymbol{k}$. For this purpose, we will first rewrite the Hamiltonian in terms of creation and annihilation operator for each energy level $\hat{H}=\sum_{i,j=1}^{4}c_i^\dagger H_{{\rm s},ij}c_j$. For a system with 2 fermions, the dimension of the Hilbert space would be 6 with the following basis:

$$\begin{aligned}&|1\rangle=c_1^\dagger c_2^\dagger|\mathrm{vac}\rangle,\ |2\rangle=c_1^\dagger c_3^\dagger|\mathrm{vac}\rangle,\\ &|3\rangle=c_1^\dagger c_4^\dagger|\mathrm{vac}\rangle,\ |4\rangle=c_2^\dagger c_3^\dagger|\mathrm{vac}\rangle,\\ &|5\rangle=c_2^\dagger c_4^\dagger|\mathrm{vac}\rangle,\ |6\rangle=c_3^\dagger c_4^\dagger|\mathrm{vac}\rangle.\end{aligned} \tag{3}$$

Here, c_i and $c_i^\dagger$ denote the fermionic annihilation and creation operator of band i, respectively. $|\mathrm{vac}\rangle$ is the vacuum state, which means there are no particles in the system. As shown in Fig. 1(b), the energy levels of the single-particle and many-particle system are plotted. In contrast to the four-fold degenerate levels with zero energy, both the levels with $E=+2\varepsilon$ and -2ε bands are not degenerate. By using the Wick theorem, the elements of Hamiltonian $\hat{H}$ in the many-particle basis $|j\rangle$ with $j=1,\ldots,6$ can be simply obtained as follows. Consider the element of the many-particle Hamiltonian $H_{\rm m,12}=\langle1|\hat{H}|2\rangle=\langle\mathrm{vac}|c_2c_1(\sum_{i,j}^{4}c_i^\dagger H_{{\rm s},ij}c_j)c_1^\dagger c_3^\dagger|\mathrm{vac}\rangle$.

One can see that only the term with $c_2^\dagger c_3$ in second quantized Hamiltonian $\hat{H}$ contributes to this element. Therefore, $H_{\mathrm{m},12} = H_{\mathrm{s},23} = h'_+$ as in Eq. (2) . Other elements of the many-particle Hamiltonian $\boldsymbol{H}_{\mathrm{m}}$ can be similarly obtained one by one. This procedure leads to a 6×6 many-particle Hamiltonian

$$\boldsymbol{H}_{\mathrm{m}} = \begin{pmatrix} 2h_0 & h'_+ & -h_+ & -h_- & -h'_- & 0 \\ h'_- & 0 & 0 & 0 & 0 & -h'_- \\ -h_- & 0 & 0 & 0 & 0 & h_- \\ -h_+ & 0 & 0 & 0 & 0 & h_+ \\ -h'_+ & 0 & 0 & 0 & 0 & h'_+ \\ 0 & -h'_+ & h_+ & h_- & h'_- & -2h_0 \end{pmatrix}. \tag{4}$$

3. Quench dynamics

In this section, we will study the quench dynamics of topological systems based on the many-particle Hamiltonian $\boldsymbol{H}_{\mathrm{m}}$. We will first study the sudden quench dynamics, in which one parameter of the Hamiltonian is suddenly changed to a new value, and the initial ground state will evolve according to the new Hamiltonian. This protocol has been well studied in the single-particle picture, and has been applied to characterize the topological phases. Then we will study the slow quench dynamics, in which one parameter is slowly changed to a new value during a finite time interval. This protocol complicates the problem. But it points out that slow quench protocol also provides a more efficient method in characterizing the topological phases.[32,33]

3.1. Sudden quench dynamics

For sudden quench, we assume the system stays initially at the ground state and then suddenly changes the Hamiltonian. We will choose h_0 as the quench axis. Initially, we assume h_0 to be infinitely large compared with other parameters, and then suddenly change h_0 to be finite value. Because the Hamiltonian is time-independent, after the sudden quench, the system will evolve according to the post-quench Hamiltonian. At an arbitrary time t, the state evolves into $|\psi(t)\rangle = \mathrm{e}^{-\mathrm{i}Ht}|\psi(0)\rangle = \sum_{j=1}^{6} a_j \mathrm{e}^{-\mathrm{i}E_j t}|j\rangle$, where a_j is the superposition coefficient of initial wave function projected on the eigenstates $|j\rangle$ of the post-quench Hamiltonian. We are interested in the experimentally measurable quantity time averaged spin polarization (TASP), which can be calculated directly by[24]

$$\overline{\langle\gamma_i\rangle} = \lim_{T\to\infty}\frac{1}{T}\int_0^T \langle\psi(t)|\gamma_i^{(\mathrm{m})}|\psi(t)\rangle\,\mathrm{d}t. \tag{5}$$

Here, $\gamma_i^{(\mathrm{m})}$ is the 6×6 many-particle counterpart of the original 4×4 single-particle Gamma matrix. To obtain $\gamma_i^{(\mathrm{m})}$, one can first write the single-particle Gamma matrix γ_i in the second quantized form as $\hat{\gamma}_i = \sum_{j,l=1}^{4} c_j^\dagger \gamma_{i,jl} c_l$. Then using the Wick theorem and following similar procedure as obtaining the many-particle Hamiltonian $\boldsymbol{H}_{\mathrm{m}}$, one can obtain the many-particle counterpart $\gamma_i^{(\mathrm{m})}$.

In the experiment of ultracold atoms, a 2D quantum anomalous Hall insulator has been realized.[25,26] By quenching the Hamiltonian from a trivial to a topological parameter regime, it is observed that a novel ring pattern of the spin dynamics emerges in momentum space during unitary evolution. The spin oscillation is quantified by measuring the momentum-dependent spin polarization with the number of atoms in the spin up and down states detected through the spin-resolved time-of-flight imaging. The resulting dynamical ring pattern can be uniquely identified to a nontrivial postquench topology. This scheme displays a high precision determination of the full phase diagram for the system's band topology.

We choose the ground state as the initial state $|\psi(0)\rangle$, i.e., $|6\rangle$. In the meanwhile, the system is quenched from a deep trivial phase to a topological nontrivial phase. Direct calculation gives a simple result of TASP

$$\overline{\langle\gamma_i\rangle} = \frac{2h_i}{\varepsilon}(|a_1|^2 - |a_6|^2), \tag{6}$$

where $a_6 = (h_0+\varepsilon)/(2\varepsilon)$, $a_1 = (h_0-\varepsilon)/(2\varepsilon)$. Aftering substituting a_6 and a_1, we readily obtain the TASP in sudden quench as follows:

$$\overline{\langle\gamma_i\rangle} = -\frac{2h_i h_0}{\varepsilon^2}. \tag{7}$$

The description of the TASP here is similar to Liu's paper, except that the value is double.[24,38]

3.2. Slow quench dynamics

In slow nonadiadatic quench, the Hamiltonian is time-dependent, i.e., $h_0(t) = h_0 + g/(2t)$ with g determining the quench rate. If g is large, the quench is slow and adiabatic. If g tends to zero, the quench reduces to the case of sudden quench. When the time t goes from 0^+ to infinity, the system undergoes a transition from a trivial phase to a topological phase. Thus, to study the slow quench dynamics and calculate the spin polarization, one needs to first solve the corresponding time-dependent Schrödinger equation with time-dependent Hamiltonian, i.e., the famous Landau–Zener problem.[32,34,35] Here, we encounter a six-state Landau–Zener problem. Exactly solvable multi-state Landau–Zener problems must satisfy integrability conditions.[34–37,40] Intriguingly, we find that this 6-state Landau–Zener problem can be exactly solved, by reducing the 6×6 Hamiltonian $\boldsymbol{H}_{\mathrm{m}}$ to an equivalent 3×3 Hamiltonian under an unitary transformation. Specifically, by introducing a unitary matrix

$$\boldsymbol{M} = \frac{1}{\sqrt{2}h}\begin{pmatrix} \sqrt{2}h & 0 & 0 & 0 & 0 & 0 \\ 0 & -\mathrm{i}h_- & -\mathrm{i}h_+ & -\mathrm{i}h'_+ & \mathrm{i}h'_- & 0 \\ 0 & -h'_+ & h'_- & h_- & h_+ & 0 \\ 0 & h_+ & -h_- & h'_- & h'_+ & 0 \\ 0 & -\mathrm{i}h'_- & -\mathrm{i}h'_+ & \mathrm{i}h_+ & -\mathrm{i}h_- & 0 \\ 0 & 0 & 0 & 0 & 0 & \sqrt{2}h \end{pmatrix},$$

with $h=\sqrt{h_1^2+h_2^2+h_3^2+h_4^2}$, one can obtain a physically equivalent Hamiltonian by an unitary transformation $\boldsymbol{H}_{\rm m}^{(6\times6)}=\boldsymbol{M}\boldsymbol{H}_{\rm m}\boldsymbol{M}^{\dagger}$

$$\boldsymbol{H}_{\rm m}^{(6\times6)}=\begin{pmatrix} 2h_0 & \sqrt{2}h & 0 & 0 & 0 & 0 \\ \sqrt{2}h & 0 & 0 & 0 & 0 & -\sqrt{2}h \\ 0 & 0 & 0 & 0 & 0 & 0 \\ 0 & 0 & 0 & 0 & 0 & 0 \\ 0 & 0 & 0 & 0 & 0 & 0 \\ 0 & -\sqrt{2}h & 0 & 0 & 0 & -2h_0 \end{pmatrix}. \tag{8}$$

Note that the unitary matrix $\boldsymbol{M}$ is independent of h_0. Therefore, this unitary transformation is always valid even for the time-dependent Hamiltonian when h_0 is time-independent.

One can see that the third, fourth and fifth levels are fully decoupled from the others, and thus an effectively 3×3 Hamiltonian is obtained. Together with the time dependent part g/t in the h_0 terms, we explicitly write down the time-dependent Hamiltonian as

$$\boldsymbol{H}_{\rm m}^{(3\times3)}(t)=\begin{pmatrix} 2h_0+g/t & \sqrt{2}h & 0 \\ \sqrt{2}h & 0 & -\sqrt{2}h \\ 0 & -\sqrt{2}h & -2h_0-g/t \end{pmatrix}. \tag{9}$$

One thus needs to solve the 3-state LZ problem

$$\mathrm{i}\partial_t|\psi(t)\rangle=\boldsymbol{H}_{\rm m}^{(3\times3)}(t)|\psi(t)\rangle. \tag{10}$$

The goal of the multistate Landau–Zener theory is to analytically determine the elements of the scattering matrix and the transition probabilities between states of this model after evolution with such a time-dependent Hamiltonian from initial time to positive infinite time. To analytically solve such a time-dependent model is a nontrivial task. Nevertheless, the results would serve as very useful tools in studying the quantum dynamics of driven systems, and provide insights in dynamical phenomena such as Kibble–Zurek mechanism,[41] quantum annealing[42] and so on. However, the exactly solvable models are rare and have been found to exist only in some special forms such as the bow-tie model[43] and time-dependent Tavis–Cumming model.[44] We will solve the three-state LZ problem (17) by investigating the intrinsic symmetry and applying the integrability constraints on the scattering amplitudes in the next section.

We note that, at initial time $t=0^+$, the time-dependent term is infinitely large and thus the ground state eigenvector is $|\psi_i\rangle=(0,0,1)^{\rm T}$. At final time $t\to\infty$, the eigenvalues are

$$E=\pm2\varepsilon,0, \tag{11}$$

with $\varepsilon=\sqrt{h_0^2+h^2}=\sqrt{\sum_{j=0}^{4}h_j^2}$, and the corresponding instantaneous eigenvectors are

$$|\psi_+\rangle=\frac{1}{2\varepsilon}\left(\varepsilon+h_0,\sqrt{2}h,h_0-\varepsilon\right)^{\rm T}, \tag{12}$$

$$|\psi_0\rangle=\frac{1}{\sqrt{2}\varepsilon}\left(h,-\sqrt{2}h_0,h\right)^{\rm T}, \tag{13}$$

$$|\psi_-\rangle=\frac{1}{2\varepsilon}\left(h_0-\varepsilon,\sqrt{2}h,h_0+\varepsilon\right)^{\rm T}. \tag{14}$$

Taking the $\mathbb{Z}_2$-type topological insulator (discussed below) as an example, we plot the instantaneous energy spectrum of $\boldsymbol{H}_{\rm m}^{(3\times3)}$ in Fig. 2(a). If the initial state is prepared in its ground state $|\psi_i\rangle=(0,0,1)^{\rm T}$ at $t\to0^+$, the system will undergo a nonadiabatic transition during time evolution governed by the time-dependent Schrödinger-equation (17). The process of this nonadiabatic transition is illustrated in Fig. 2(b), showing the occupation probability of the $|\psi(t)\rangle$ on three instantaneous eigenvectors as a function of time t. Starting from the initial state $|\psi_i\rangle$ with unit probability, the energy gap of the system gradually becomes smaller, and in the meanwhile, the occupation probability of $|\psi(t)\rangle$ on instantaneous ground eigenvectors decreases, while the probability on the others two instantaneous eigenvectors increase. At the long time limit, the energy gap remains as a constant and corresponding occupation probability on each energy level arrives at its saturation value.

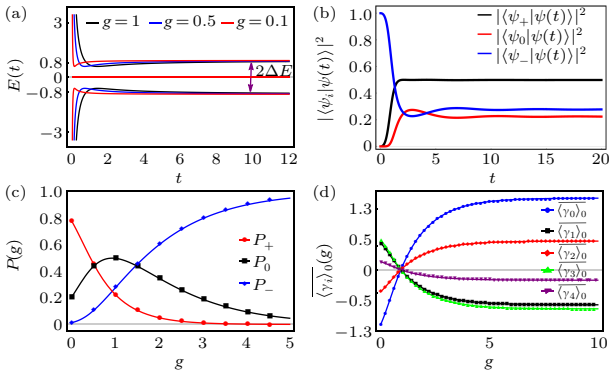


Fig. 2. (a) The instantaneous eigenvalue as a function of time t for different values of g. Here, we choose the point $(k_x,k_y)=(2\pi/3,-\pi/4)$ in the model (40) with parameters $m=-0.5t_0$, $t_0'=0.5t_0$, $t_{\rm so}=0.2t_0$. (b) Occupation probability of the state vector $|\psi(t)\rangle$ on three instantaneous eigenvectors with $g=1$. (c) Transition probability P from initial ground state to final state as a function of g. These colored points and solid lines are numerical results and analytic results, respectively. The analytic results are given by Eqs. (35)–(38). In the numerics, time t is taken from 0.0001 to 20000. (d) TASP as functions of varying g.

In Fig. 2(c), we plot the transition probability P_-, P_0 and P_+ of the initial ground state $|\psi_i\rangle=(0,0,1)^{\rm T}$ to the final three eigenvectors $|\psi_-\rangle$, $|\psi_0\rangle$ and $|\psi_+\rangle$ at $t\to\infty$, respectively. Numerical simulations and analytical results agree with each other. One can see the system experiences a transition from nonadiabatic evolution to adiabatic evolution while varying g from 0 to ∞. When g is small, the transition is nonadiabatic and is close to the sudden quench limit with most of the probability on the final up state. As g becomes larger, the dynamics becomes adiabatic and the system can follow the instantaneous ground state with increasing P_-.

Based on the Landau–Zener probability, one can write down the final state vector at long-time limit

$$|\psi(t)\rangle=\sqrt{P_+}\,\mathrm{e}^{-\mathrm{i}2\varepsilon t+\delta_1}|\psi_+\rangle+\sqrt{P_-}\,\mathrm{e}^{\mathrm{i}2\varepsilon t+\delta_2}|\psi_-\rangle$$

$$+\sqrt{P_0}|\psi_0\rangle, \tag{15}$$

where δ_1 and δ_2 are two undetermined relative phase factors.

Furthermore, one can study the dynamics of spin polarization $\langle\boldsymbol{\gamma}(t)\rangle = \langle\psi(t)|\boldsymbol{\gamma}|\psi(t)\rangle$ and its average (TASP) after a long time period of evolution

$$\overline{\langle\gamma_i\rangle} = \frac{2h_i}{\varepsilon}(P_+ - P_-). \tag{16}$$

This result agrees well with the results of numerical simulation as shown in Fig. 2(d). When $g \to 0$, this solution is also the TASP of sudden quench. Here, we define the position $(P_+ - P_-) = 0$ as SIS.[32,33]

Before discussing the specific topological models, it should be mentioned that the nonadiabatic protocol is readily accessible in ultracold atomic experiments by using a bias magnetic field to simulate the time-changing part of the quenching axis.[25,26] Furthermore, the spin polarization can be measured by using the spin-resolved time-of-flight imaging. Moreover, the nonadiabatic transition time t_c can be estimated as $t_c \sim \hbar/\Delta$, which is of the order of 10 μs. Here, Δ is the characteristic energy scale. In order to observe the effect of the nonadiabatic transition in experiment, the nonadiabatic transition time t_c must be much smaller than the decoherence time τ of the ultracold atomic system, which is longer than 1 ms. Therefore, this condition is satisfied and the nonadiabatic quench protocol is quite promising in detecting the topological phases in ultracold atoms.

4. Exact solution of the three-level Landau–Zener problem

Before we apply the slow quench dynamics to the dynamical characterization of topological phases, we provide the exactly analytical solution of the new three-state Landau–Zener model we obtained in previous section. Explicitly, the time-dependent Schrödinger equation is

$$\mathrm{i}\frac{\mathrm{d}}{\mathrm{d}t}|\psi(t)\rangle = \boldsymbol{H}(t)|\psi(t)\rangle, \tag{17}$$

with

$$\boldsymbol{H}(t) = \begin{pmatrix} 2h_0 + g/t & \sqrt{2}h & 0 \\ \sqrt{2}h & 0 & -\sqrt{2}h \\ 0 & -\sqrt{2}h & -2h_0 - g/t \end{pmatrix}. \tag{18}$$

The time t is from 0^+ to ∞. At initial time, the instantaneous eigenvalues are ∞, 0, and $-\infty$, which we denote as 1, 2 and 3 levels. At final time $t = \infty$, the instantaneous eigenvalues are $\pm 2\varepsilon$ and 0 with eigenvectors given in Eqs. (12)–(14), which we denote as $\pm$, and 0 levels, respectively. We define transition probability $P_{\mu j}$ and the corresponding scattering matrix $\hat{\boldsymbol{S}}_+$ with elements $\hat{S}_{\mu j}$ from initial j-th level to final μ-th level, with $j = 1,2,3$, and $\mu = +,0,-$. Clearly, one has $P_{\mu j} = |\hat{S}_{\mu j}|^2$. We explicitly write down the scattering matrix[46,47]

$$\hat{\boldsymbol{S}}_+ = \begin{pmatrix} s_{+1} & s_{+2} & s_{+3} \\ s_{01} & s_{02} & s_{03} \\ s_{-1} & s_{-2} & s_{-3} \end{pmatrix}. \tag{19}$$

Note that the Schrödinger equation (17) possesses a chiral symmetry. If we write $\psi(t) = (a_1, a_2, a_3)^{\mathrm{T}}$, Eq. (17) is invariant when exchanging a_1 and a_3 together with taking the conjugate so that $\mathrm{i} \to -\mathrm{i}$, or $\hat{\boldsymbol{H}} \to -\hat{\boldsymbol{H}}$. This joint operation produces a new scattering matrix $\hat{\boldsymbol{S}}'_+$. On the one hand, the elements of $\hat{\boldsymbol{S}}'_+$ can be obtained from $\hat{\boldsymbol{S}}_+$ by exchanging the indexes $1 \to 3$ and $+ \to -$, i.e.,

$$\hat{\boldsymbol{S}}'_+ = \begin{pmatrix} s_{-3} & s_{-2} & s_{-1} \\ s_{03} & s_{02} & s_{01} \\ s_{+3} & s_{+2} & s_{+1} \end{pmatrix}. \tag{20}$$

On the other hand, the two scattering matrices are related with each other through a conjugate operation $\hat{\boldsymbol{S}}'_+ = \hat{\boldsymbol{S}}^*_+$. Therefore we have several identities $s_{-3} = s^*_{+1}$, $s_{-2} = s^*_{+2}$, $s_{+3} = s^*_{-1}$, $s_{03} = s^*_{01}$ and $s_{02} = s^*_{02}$. Explicitly, these identities reduce Eq. (19) to be

$$\hat{\boldsymbol{S}}_+ = \begin{pmatrix} s_{+1} & s_{+2} & s^*_{-1} \\ s_{01} & s_{02} & s^*_{01} \\ s_{-1} & s^*_{+2} & s^*_{+1} \end{pmatrix}. \tag{21}$$

Also, s_{02} is real.

We also have the unitary condition of $\hat{\boldsymbol{S}}_+$, $\hat{\boldsymbol{S}}^\dagger_+\hat{\boldsymbol{S}}_+ = \hat{1}$, which gives rise to more conditions

$$|s_{+1}|^2 + |s_{+2}|^2 + |s_{-1}|^2 = 1, \tag{22}$$

$$2|s_{01}|^2 + |s_{02}|^2 = 1, \tag{23}$$

$$2|s_{12}|^2 + |s_{02}|^2 = 1, \tag{24}$$

$$2s_{+1}s^*_{-1} + s^2_{+2} = 0. \tag{25}$$

From Eqs. (23) and (24), one obtains $|s_{01}| = |s_{12}|$. From Eq. (25) one obtains $|s_{+2}|^2 = 2|s_{+1}||s_{-1}|$. Substituting this relation into Eq. (22), one can get $|s_{+1}| + |s_{-1}| = 1$. Returning to the transition probability

$$\hat{\boldsymbol{P}} = \begin{pmatrix} P_{+1} & P_{01} & P_{-1} \\ P_{01} & P_{02} & P_{01} \\ P_{-1} & P_{01} & P_{+1} \end{pmatrix}, \tag{26}$$

with relations

$$P_{+1} + P_{01} + P_{-1} = 1, \tag{27}$$

$$2P_{01} + P_{02} = 1, \tag{28}$$

$$\sqrt{P_{+1}} + \sqrt{P_{-1}} = 1. \tag{29}$$

Now we have 4 parameters to be determined, but only 3 conditions. One more condition is yet to be established.

We resort to the connection formula.[46] First we make an unitary transformation to the Hamiltonian such that, in the

new basis, the Hamiltonian has a form of $\hat{\boldsymbol{A}}+\hat{C}/t$ with the constant matrix $\hat{\boldsymbol{A}}$ being diagonal. The unitary matrix is

$$\hat{\boldsymbol{V}}=\frac{1}{2\varepsilon}\begin{pmatrix} h_0+\varepsilon & \sqrt{2}h & h_0-\varepsilon \\ \sqrt{2}h & -2h_0 & \sqrt{2}h \\ h_0-\varepsilon & \sqrt{2}h & h_0+\varepsilon \end{pmatrix}. \tag{30}$$

The new Hamiltonian $\boldsymbol{H}'=\hat{\boldsymbol{V}}\boldsymbol{H}(t)\hat{\boldsymbol{V}}^{\dagger}$ is

$$\boldsymbol{H}'=\begin{pmatrix} 2\varepsilon+g_0/t & g_h/t & 0 \\ g_h/t & 0 & -g_h/t \\ 0 & -g_h/t & -2\varepsilon \end{pmatrix}, \tag{31}$$

with $g_0=gh_0/\varepsilon$ and $g_h=gh/\sqrt{2}\varepsilon$. It has been pointed out that, for a Schrödinger equation like the form of

$$\mathrm{i}\partial_t\psi=(\hat{\boldsymbol{A}}+\hat{C}/t)\psi, \tag{32}$$

it is equivalent to a Schrödinger equation like

$$\mathrm{i}\partial_\tau\psi=(\hat{\boldsymbol{A}}\tau+2\hat{C}/\tau)\psi, \tag{33}$$

which can be obtained by a change of variable: $t=\tau^2/2$. For Eq. (33), the equation is symmetry under time reversal $\tau\to-\tau$. Denoting the scattering matrix of Eq. (33) from $\tau=0^+$ to ∞ as $\hat{\boldsymbol{S}}_+$, and the scattering matrix from $\tau=-\infty$ to 0^- as $\hat{\boldsymbol{S}}_-$, the time reversal symmetric guarantees that $\hat{\boldsymbol{S}}_-=\hat{\boldsymbol{S}}_+^{\dagger}$. In the complex plane of time, one can draw a semicircle $\mathcal{C}_+$ with infinite radius in the upper plane connecting the time $\tau=-\infty$ to ∞. Along this contour $\mathcal{C}_+$, the element S_{11}^{up} in the scattering matrix is given as $S_{11}^{\mathrm{up}}=\mathrm{e}^{-\pi g_0}$. This scattering element should be equal to the one along the real axis $t\in(-\infty,0^-)$ and $t\in(0^+,\infty)$ connected by a small semicircle $\mathcal{C}_0$ around the original point, i.e., $[\hat{\boldsymbol{S}}_+\hat{S}_0^{\mathrm{up}}\hat{\boldsymbol{S}}_-]_{11}=S_{11}^{\mathrm{up}}$. Here, $\hat{S}_0^{\mathrm{up}}$ is the scattering matrix of the small contour $\mathcal{C}_0$, and up denotes that contour $\mathcal{C}_0$ is in the upper plane. This connection formula gives the following identity:[46]

$$\mathrm{e}^{-2\pi g}P_{+1}+P_{01}+\mathrm{e}^{2\pi g}P_{-1}=\mathrm{e}^{-2\pi g h_0/\varepsilon}. \tag{34}$$

Now we have four parameters to be determined in Eq. (26) and also four identities. Therefore the transition probability can be determined unambiguously

$$P_{+1}=\left(\frac{\mathrm{e}^{\pi g}-\mathrm{e}^{-\pi g_{\mathrm{c}}}}{\mathrm{e}^{\pi g}-\mathrm{e}^{-\pi g}}\right)^2, \tag{35}$$

$$P_{01}=2\frac{(\mathrm{e}^{\pi(g-g_{\mathrm{c}})}-1)(1-\mathrm{e}^{-\pi(g+g_{\mathrm{c}})})}{(\mathrm{e}^{\pi g}-\mathrm{e}^{-\pi g})^2}, \tag{36}$$

$$P_{-1}=\left(\frac{\mathrm{e}^{-\pi g_{\mathrm{c}}}-\mathrm{e}^{-\pi g}}{\mathrm{e}^{\pi g}-\mathrm{e}^{-\pi g}}\right)^2, \tag{37}$$

$$P_{02}=\left(\frac{\mathrm{e}^{\pi g}+\mathrm{e}^{-\pi g}-2\mathrm{e}^{-\pi g_{\mathrm{c}}}}{\mathrm{e}^{\pi g}-\mathrm{e}^{-\pi g}}\right)^2, \tag{38}$$

with

$$g_{\mathrm{c}}=g\frac{h_0}{\varepsilon}. \tag{39}$$

Note that the transition probabilities P_{+1}, P_{01} and P_{-1} are those from the initial ground state to the three final states $|+\rangle$, $|0\rangle$ and $|-\rangle$. Therefore, they are just the three quantities P_+, P_0 and P_- in the previous section.

5. The nonadiabatic characterization of topological phases

Now, we can apply the obtained TASP to the dynamical topological characterization of the real models. The Hamiltonian $\boldsymbol{H}_{\mathrm{s}}$ which we considered in this paper can describe at least two different topological phases. When $h_4\neq0$, $\boldsymbol{H}_{\mathrm{s}}$ corresponds to the $\mathbb{Z}_2$ topological insulators, including the 3D first descendant and 2D second descendant insulators. When $h_4=0$, $\boldsymbol{H}_{\mathrm{f}}$ corresponds to the 3D chiral topological insulators. The dynamical characterization of the 3D chiral topological insulators only needs the introduction of 1-BIS and 1-SIS (low-order), while the characterization of the $\mathbb{Z}_2$ topological insulators needs the introduction of high-order BIS and high-order SIS.[33]

5.1. $\mathbb{Z}_2$-type topological insulator

As an example of characterizing $\mathbb{Z}_2$ topological insulator, a 2D $\mathbb{Z}_2$ topological phase[38] is considered with Hamiltonian

$$\begin{aligned} h_0&=\frac{g}{2t}+m-t_0\sum_{i=x,y}\cos k_i-t_0'\sum_{i=1,2}\cos[k_x-(-1)^i k_y], \\ h_{1,2}&=t_{\mathrm{so}}\sin k_{x,y},\quad h_{3,4}=t_{\mathrm{so}}\sin[k_x\pm k_y], \end{aligned} \tag{40}$$

where t_0,t_0' represent the spin-conserved hopping coefficients while t_{so} denotes the spin-flipped hopping coefficients. The equilibrium topology of this model is characterized by the value of m with the Fu–Kane invariant $\mathrm{FK}=\mathrm{sgn}\{(m+2t_0')^2[(m-2t_0')^2-4t_0^2]\}$.[48,49]

By slowly quenching h_0 from $t=0$ to $t=\infty$ with $m=-0.5$, five components of TASP are observed as shown in Fig. 3. As one can see, 1D 3-BIS and 1D 3-SIS with vanished spin polarization are observed in $\overline{\langle\gamma_0\rangle}$, and their corresponding position in other components of TASP are denoted by purple dashed ring and green dashed ring, respectively. Moreover, the 0D 4-BIS and 0D 4-SIS can be easily constructed on 3-SIS and 3-BIS by the intersection of vanishing polarization between two components of TASP. Here we choose $\overline{\langle\gamma_0\rangle}\cap\overline{\langle\gamma_2\rangle}=0$ as an example. As shown in Figs. 3(a) and 3(c), the 0D 4-BIS and 0D 4-SIS are indicated by the purple points and green points, respectively. To give an intuitive comprehension of the behaviour of 4-BIS and 4-SIS, we also plot the time evolution of five components $\langle\gamma_{0,1,2,3,4}\rangle$ on 4-BIS, 4-SIS and other point in Fig. 4. The spin at each $\boldsymbol{k}$ point precesses after quenching system from a fully spin-polarized state pointing along negative h_0 axis. One can observe an approximately stable dynamic precession behavior of spin polarization on all three points after a short period of evolution. For 4-BIS points in Fig. 4(b), after a certain time t ($t\gg g$), the fields along the h_1 and h_3,

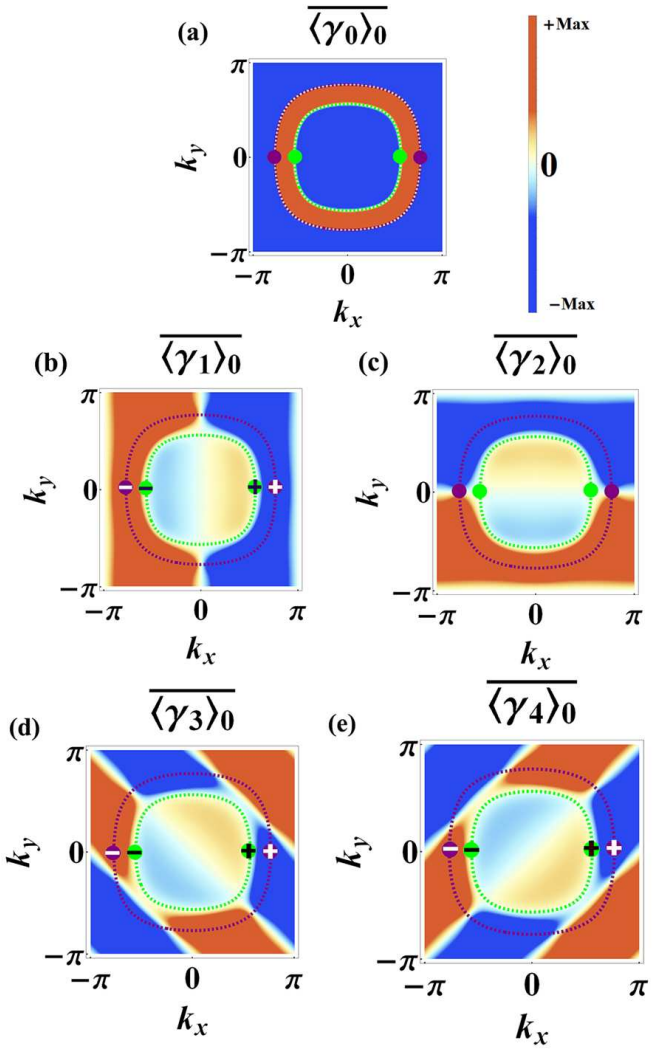


Fig. 3. Analytical results of TASP under slow quench dynamics. The system is quenched from $t=0$ to $t=\infty$ with $5t_{so}=2t_0'=-2m=t_0=1, g=5$. After quenching h_0, five components of TASP are shown. The 3-BIS and 3-SIS are denoted by purple dashed lines and green dashed lines, respectively. The opposite signs on 4-BIS (4-SIS) constructed by $\overline{\langle\gamma_{0,2}\rangle}$ in $\overline{\langle\gamma_{1,3,4}\rangle}$ characterizes the nontrivial topology, and implies the $\mathbb{Z}_2$ invariant $\nu^{(2)}=-1$.

and h_4 are nonzero and equal with each other, while both the fields along the h_0, h_2 are zero. Thus, one can see $\overline{\langle\gamma_{1,3,4}\rangle}$ always a nonzero value. In addition, due to the strong polarization of initial state, the $\langle\gamma_0\rangle$ oscillates between positive and negative values, while the $\langle\gamma_2\rangle$ is always zero. Thus, both $\overline{\langle\gamma_{0,2}\rangle}$ are always zero. For 4-SIS in Fig. 4(c), the polarizations $\langle\gamma_{0,1,3,4}\rangle$ undergo a resonant spin-reversing transitions, and thus $\overline{\langle\gamma_{0,1,3,4}\rangle}=0$. In addition, due to the disapperance of the field along the h_2 axis, the polarization $\overline{\langle\gamma_2\rangle}$ is still zero. These features can be convenient to identify the position of SIS and BIS based on TASP in experiments. In addition, all the components of spin polarization of a general point do not oscillate between positive and negative values, and thus have no distinguished features in TASP. We can see from Eqs. (16) and (40) that at $t\to 0$, since h_0 has a g/t term and others do not. So, as $t\to 0$, only $\langle\gamma_0\rangle$ has a value, and $\langle\gamma_{1,2,3,4}\rangle$ approaches to 0. And after a long time of evolution, all the components into a relatively stable periodic oscillation. However, for BIS, there is only $\langle\gamma_0\rangle$ oscillating between positive and negative values. Thus, the long-time averaged value of $\langle\gamma_0\rangle$ will vanish, while other components of TASP are still nonzero. Compared with BIS, $\langle\gamma_{0,1,3,4}\rangle$ all oscillates on SIS between positive and negative values, corresponding to a vanishing spin polarization in all components of TASP. These features can be convenient to identify the position of SIS and BIS based on TASP in experiments. In addition, all the components of spin polarization of a general point do not oscillate between positive and negative values, and thus have no distinguished features in TASP.

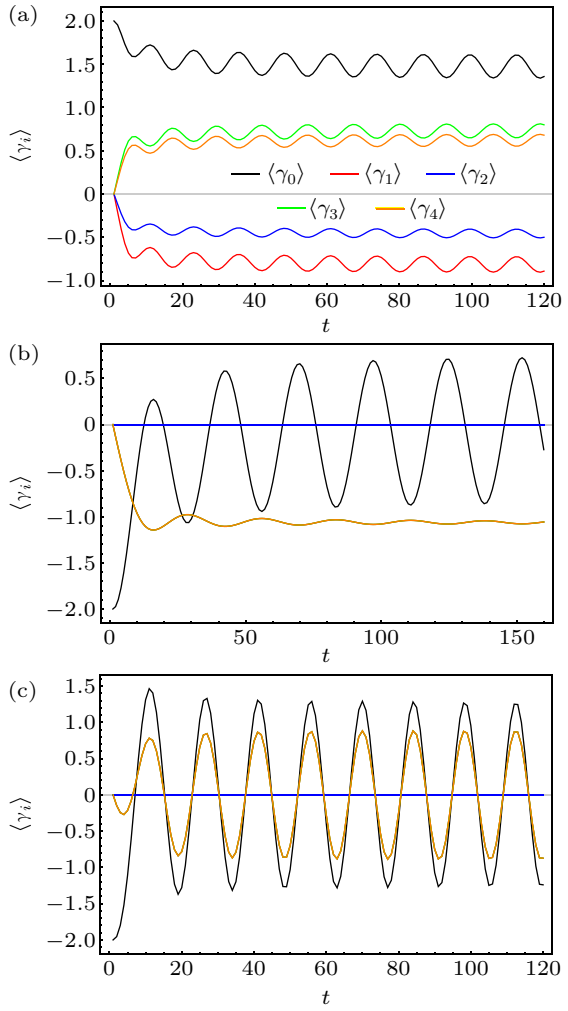


Fig. 4. Analytical results of time evolution of spin polarization for 2D $\mathbb{Z}_2$ topological model after slow quenching h_0 axis with $t_{so}=0.2$, $m=-0.5$, $t_0'=0.5$, $t_0=g=1$. (a) The corresponding time evolution of spin polarization on a general point, (b) 4-BIS and (c) 4-SIS, respectively. In panels (b) and (c), $\overline{\langle\gamma_1\rangle}$, $\overline{\langle\gamma_3\rangle}$ and $\overline{\langle\gamma_4\rangle}$ are superimposed.

The values of 0D 4-BIS and gradients of 0D 4-SIS are indicated by the opposite signs as shown in Figs. 3(b), 3(d) and 3(e), implying the nontrivial $\mathbb{Z}_2$ index $\nu^{(2)}=-1$. Specifically, on 4-BIS, we can see that the values of $-\overline{\langle\gamma_{1,3,4}\rangle}$ are -1 at negative k_x point and $+1$ at positive k_x point, as marked by the white opposite signs $+$ and $-$ in $\overline{\langle\gamma_{1,3,4}\rangle}$, respectively. The nontrivial topological invariant can then be obtained by $\nu^{(2)}=\frac{1}{2}[\mathrm{sgn}(-\overline{\langle\gamma_{1,3,4}\rangle}_{k_{x,-}})-\mathrm{sgn}(-\overline{\langle\gamma_{1,3,4}\rangle}_{k_{x,+}})]=-1$. On 4-

SIS, we can see that the values of gradients $\tilde{g}_{1,3,4}$ are -1 at negative k_x point and $+1$ at positive k_x point, as marked by the black opposite signs $+$ and $-$ in $\overline{\langle\gamma_{1,3,4}\rangle}$, respectively. The value of topological invariant can then be obtained by $\nu^{(2)} = \frac{1}{2}[\mathrm{sgn}(\tilde{g}_{1,3,4,k_{x,-}}) - \mathrm{sgn}(\tilde{g}_{1,3,4,k_{x,+}})] = -1$.

5.2. $\mathbb{Z}$-type topological insulator

We proceed to give the characterization scheme of the high-dimensional $\mathbb{Z}$-type topological phases under slow nonadiabatic quench dynamics. The Hamiltonian of 3D topological phase can be written as $\boldsymbol{H}(k) = \sum_{i=0}^{4} h_i \gamma_i$, with

$$h_0 = \frac{g}{2t} + m - t_0 \sum_{j=x,y,z} \cos k_i,$$
$$h_{1,2,3} = t_{\mathrm{so}} \sin k_{x,y,z}, \quad h_4 = 0. \tag{41}$$

We quench this system from $t = 0^+$ to $t \to \infty$ with large m to a finite value, and thus the system finally lies in different phases depending on the value of m: for $|m| > 3t_0$, the trivial phase; for $t_0 < m < 3t_0$, the topological phase with winding number $\nu_3 = -1$; for $-t_0 < m < t_0$ with $\nu_3 = 2$, and for $-3t_0 < m < -t_0$, with $\nu_3 = -1$.

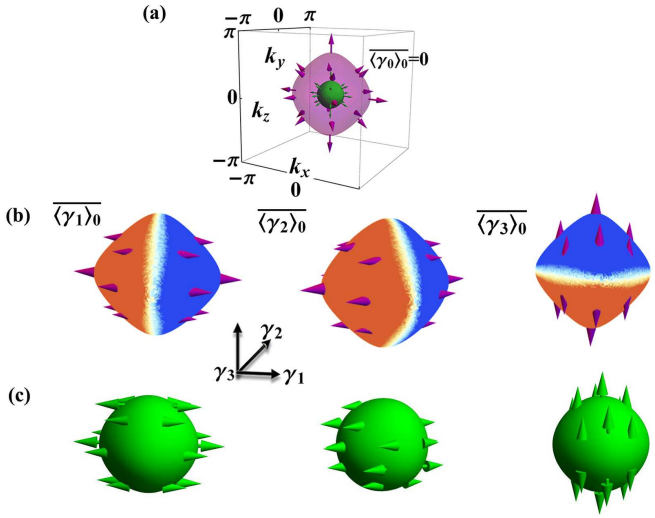


Fig. 5. Analytical results of TASP for the 3D chiral topological insulator under slow quench dynamics. Here we set $t_{\mathrm{so}} = t_0 = g = 1$, $m = 1.5$. In panel (a), the purple surface is 1-BIS which is defined by $\overline{\langle\gamma_0\rangle} = 0$, and the purple arrows are the dynamical field shown in panel (b). The green one is SIS, and the green arrows are the dynamical field shown in panel (c). In panels (b) and (c), the three components of TASP $\overline{\langle\gamma_{1,2,3}\rangle}$ on 1-BIS and 1-SIS are shown. The dynamical field $-\overline{\langle\gamma_{1,2,3}\rangle}$ and $\widetilde{g_{1,2,3}}$ are illustrated by purple and green arrows, respectively.

As shown in Fig. 5(a), one can see both BIS and SIS (purple and green surfaces) become a closed surfaces where spin polarization vanished in $\overline{\langle\gamma_0\rangle} = 0$. In Fig. 5(b), the non-zero values of spin polarization $-\overline{\langle\gamma_1\rangle}$, $-\overline{\langle\gamma_2\rangle}$, $-\overline{\langle\gamma_3\rangle}$ on the corresponding BIS are plotted by the purple arrows, and then combined into the BIS in $\overline{\langle\gamma_0\rangle}$. The above combined purple arrows display a three-dimensional topological pattern on the BIS surface, and thus give a nontrivial winding number $\nu_3 = 1$. In addition, the topological characterization of SIS is similar as that of BIS, except that the dynamical field $-\overline{\langle\gamma_{1,2,3}\rangle}$ is replaced by gradient $\widetilde{g_{1,2,3}}$, which is also proportional to the $h_{1,2,3}$. As shown in Fig. 5(b), the non-zero values of these gradients $\widetilde{g_{1,2,3}}$ on the corresponding SIS of $-\overline{\langle\gamma_{1,2,3}\rangle}$ are plotted by the green arrows, and then combine to the SIS in $\overline{\langle\gamma_0\rangle}$. The above combined green arrows also display a three-dimensional topological pattern on the SIS surface, which also correspond to 3D phases with winding number $\nu_3 = 1$.

6. Discussion

In previous sections, we consider only the Hamiltonian expressed in terms of Gamma matrices that anticommute with each other. In this case, the eigenvalues are doubly degenerate. That is the reason why the result of half-filled case is simply double of the single-particle case. If one adds a symmetry-breaking term in the original Hamiltonian, the double degeneracy would be lifted. Taking the following term as an example:

$$\boldsymbol{H}_{\mathrm{sb}} = h_5 \boldsymbol{\sigma}_0 \otimes \boldsymbol{\sigma}_z, \tag{42}$$

the eigenvalues of the total Hamiltonian split into four non-degenerate energy levels. In this case, only considering the single-particle dynamics from the ground state would not be comparable to experiment in which the two valence bands are both occupied, and the two have different dynamics. However, with the breaking-symmetry term, no analytical solution can be found for the Landau–Zener problem. The corresponding 6×6 many-particle Hamiltonian can not be reduced to a simpler 3×3 Hamiltonian.

The main purpose of this work is to study non-interacting system with two valence bands fully occupied, which serves as a starting point for the future research considering the interaction effects. The inclusion of interaction, even the simplest case of on-site Hubbard interaction would severely complicate the problem, and may induce various interesting quantum phases such as superfluid phase and antiferromagnetic phase.[50,51] However, the result of our work without interaction may still be useful and give some instructions in the case with weak interaction. Here taking the on-site Hubbard interaction as an example, we will briefly outline the framework of solving slow quench dynamics. The starting point may be the 2D Kane–Mele–Hubbard model with Hamiltonian[50,51]

$$H = \sum_{\boldsymbol{k}} C_{\boldsymbol{k}}^{\dagger} \mathcal{H}_{\boldsymbol{k}}^{(0)} C_{\boldsymbol{k}} + U \sum_{\boldsymbol{j},\alpha=A,B} n_{\alpha,\boldsymbol{j}\uparrow} n_{\alpha,\boldsymbol{j}\downarrow}, \tag{43}$$

where $C_{\boldsymbol{k}} = (c_{A\boldsymbol{k}\uparrow}, c_{B\boldsymbol{k}\downarrow}, c_{A\boldsymbol{k}\downarrow}, c_{B\boldsymbol{k}\uparrow})^{\mathrm{T}}$ is the spinor operator of momentum $\boldsymbol{k}$, $n_{\alpha,j,s} = c_{\alpha,j,s}^{\dagger} c_{\alpha,j,s}$ is the particle number operator at site $\boldsymbol{j}$ and sublattice α with $\alpha = A, B$ and $s = \uparrow, \downarrow$. The non-interacting Hamiltonian $\mathcal{H}^{(0)}$ is given by Eq. (40). In the 2D case, the Hubbard interaction can be treated within mean-field theory with the fluctuations neglected. This approximation has been shown to be valid in the weak interaction limit

and one can focus on the ferromagnetic order. Accordingly, the Hubbard interaction term can be rewritten as

$$\sum_{\boldsymbol{j}} n_{\alpha,\boldsymbol{j},\uparrow} n_{\alpha,\boldsymbol{j},\downarrow} = n_{\alpha\uparrow} \sum_{\boldsymbol{k}} c^{\dagger}_{\alpha\boldsymbol{k}\downarrow} c_{\alpha\boldsymbol{k}\downarrow} + n_{\alpha\downarrow} \sum_{\boldsymbol{k}} c^{\dagger}_{\alpha\boldsymbol{k}\uparrow} c_{\alpha\boldsymbol{k}\uparrow} - N n_{\alpha\uparrow} n_{\alpha\downarrow}, \tag{44}$$

where $n_{\alpha\mathrm{s}} = (1/N)\sum_{\boldsymbol{k}} \langle c^{\dagger}_{\alpha\boldsymbol{k}\mathrm{s}} c_{\alpha\boldsymbol{k}\mathrm{s}} \rangle$ with N being the total number of sites. Under mean field theory, it is clear that one has to self-consistently calculate the four particle densities $n_{\alpha\mathrm{s}}$, which vary with time in the nonadiabatic transition. Meanwhile, the time-dependent Hamiltonian now contains not only the driving term g/t, but also the time-varying particle densities $n_{\alpha\mathrm{s}}(t)$. It would be interesting to develop an efficient method to perform this time-dependent self-consistent calculation in the future research.

7. Conclusion

We have studied the many-body dynamical characterization of topological phases with a focus on whether the Pauli exclusion principle would affect the transition probability after slow quench dynamics. By investigating the TASP of many-particle fermionic systems under nonadiabatic quench dynamics, we find that the TASP of many-particle is the algebraic sum of the single-particle system. Albeit simple, this result is quite nontrivial as considering the Pauli exclusion principle so that, in the time-evolution, different particles would effectively repel each other. Moreover, to achieve the results, we have obtained a new three-level Landau–Zener model which adds to the class of exactly solvable models. This nontrivial model is solved by investigating the intrinsic symmetry of the time-dependent Hamiltonian and by applying the integrability conditions. The obtained TASP (also confirmed numerically) can be applied to characterize the bulk topology of system in nonequilibrium state. Furthermore, our results suggest a general method for exploring the band topology of noninteracting many-particle fermionic systems. Particularly, it is worthwhile to notice that the nonadiabatic quench can be realized in ultracold atomic experiments because the nonadiabatic transition time t_{c} much smaller than the decoherence time of the ultracold atomic system τ. Thus, one can expect our results may provide reference in future experiment of (super)weak interaction.

Appendix A

In this appendix, we provide details of obtaining the unitary matrix $\boldsymbol{M}$ in reducing the 6×6 many-particle Hamiltonian $\boldsymbol{H}_{\mathrm{m}}$ to the 3×3 Hamiltonian $\boldsymbol{H}^{(3\times 3)}$.

Starting from the 6×6 Hamiltonian $\boldsymbol{H}_{\mathrm{m}}$ (4), we first change the order of the second through fifth columns so that the Hamiltonian looks like the following:

$$\boldsymbol{H}_1 = \begin{pmatrix} 2h_0 & h_+ & h_- & h'_+ & h'_- & 0 \\ h_- & 0 & 0 & 0 & 0 & -h_- \\ h_+ & 0 & 0 & 0 & 0 & -h_+ \\ h'_- & 0 & 0 & 0 & 0 & -h'_- \\ h'_+ & 0 & 0 & 0 & 0 & -h'_+ \\ 0 & -h_+ & -h_- & -h'_+ & -h'_- & -2h_0 \end{pmatrix}. \tag{A1}$$

The corresponding unitary matrix is

$$\boldsymbol{T}_1 = \begin{pmatrix} 1 & 0 & 0 & 0 & 0 & 0 \\ 0 & 0 & -1 & 0 & 0 & 0 \\ 0 & 0 & 0 & -1 & 0 & 0 \\ 0 & 1 & 0 & 0 & 0 & 0 \\ 0 & 0 & 0 & 0 & -1 & 0 \\ 0 & 0 & 0 & 0 & 0 & 1 \end{pmatrix}. \tag{A2}$$

The second step is to introduce a unitary transformation $\boldsymbol{T}_2$ to make the second to fifth columns look more simpler

$$\boldsymbol{T}_2 = \begin{pmatrix} 1 & 0 & 0 & 0 & 0 & 0 \\ 0 & \frac{1}{\sqrt{2}} & \frac{1}{\sqrt{2}} & 0 & 0 & 0 \\ 0 & \frac{\mathrm{i}}{\sqrt{2}} & -\frac{\mathrm{i}}{\sqrt{2}} & 0 & 0 & 0 \\ 0 & 0 & 0 & \frac{1}{\sqrt{2}} & \frac{1}{\sqrt{2}} & 0 \\ 0 & 0 & 0 & \frac{\mathrm{i}}{\sqrt{2}} & -\frac{\mathrm{i}}{\sqrt{2}} & 0 \\ 0 & 0 & 0 & 0 & 0 & 1 \end{pmatrix}. \tag{A3}$$

Making the unitary transformation $\boldsymbol{H}'_{\mathrm{m}} = \boldsymbol{T}_2 \boldsymbol{H}_{\mathrm{m}} \boldsymbol{T}_2^{\dagger}$, we have

$$\boldsymbol{H}_2 = \sqrt{2} \begin{pmatrix} \sqrt{2}h_0 & h_1 & h_2 & h_3 & h_4 & 0 \\ h_1 & 0 & 0 & 0 & 0 & -h_1 \\ h_2 & 0 & 0 & 0 & 0 & -h_2 \\ h_3 & 0 & 0 & 0 & 0 & -h_3 \\ h_4 & 0 & 0 & 0 & 0 & -h_4 \\ 0 & -h_1 & -h_2 & -h_3 & -h_4 & -\sqrt{2}h_0 \end{pmatrix}, \tag{A4}$$

which displays a very symmetric pattern in the second to fifth columns and rows. One can thus try the following unitary matrix:

$$\boldsymbol{T}_3 = \frac{1}{h} \begin{pmatrix} h & 0 & 0 & 0 & 0 & 0 \\ 0 & h_1 & h_2 & h_3 & h_4 & 0 \\ 0 & h_2 & -h_1 & -h_4 & h_3 & 0 \\ 0 & h_3 & h_4 & -h_1 & -h_2 & 0 \\ 0 & h_4 & -h_3 & h_2 & -h_1 & 0 \\ 0 & 0 & 0 & 0 & 0 & h \end{pmatrix}. \tag{A5}$$

In this way, we obtain the matrix $\boldsymbol{H}_{\mathrm{m}}^{(6\times 6)}$ (8), and the total unitary transformation is $\boldsymbol{M} = \boldsymbol{T}_3 \boldsymbol{T}_2 \boldsymbol{T}_1$.

The reason why we can reduce the 6×6 matrix is rooted in the symmetries possessed by original 4×4 Hamiltonian. We note that the original 4×4 Hamiltonian is expressed in terms of Gamma matrices that anticommute with each other

$$\boldsymbol{H}_{\mathrm{s}} = \sum_{j=0}^{4} h_j \gamma_j. \tag{A6}$$

Here, h_j is the components of effective field, and $\boldsymbol{\gamma}_j$ is 4×4 matrices and obeys the Clifford algebra $\{\boldsymbol{\gamma}_j, \boldsymbol{\gamma}_l\} = 2\boldsymbol{\delta}_{jl}$ for $j,l = 0,1,\ldots,4$. Without loss of generality, we choose the following convention for Gamma matrices: $\boldsymbol{\gamma}_0 = \boldsymbol{\sigma}_z \otimes \boldsymbol{\sigma}_0$,

$\gamma_1 = \sigma_x \otimes \sigma_z$, $\gamma_2 = \sigma_y \otimes \sigma_0$, $\gamma_3 = \sigma_x \otimes \sigma_x$, $\gamma_4 = \sigma_x \otimes \sigma_y$, with $\sigma_{x,y,z}$ being the three Pauli matrices and σ_0 being the 2×2 identity matrix. This Hamiltonian has eigenvalues that are doubly degenerate: $E_\pm = \pm\varepsilon$ with $\varepsilon = \sqrt{\sum_{j=0}^{d} h_j^2}$. This is the result of the symmetries of the Hamiltonian. Due to the anticommutation relation of Gamma matrices, we have

$$\gamma_j \boldsymbol{H}_{\rm s}(h_j)\gamma_j = -\boldsymbol{H}_{\rm s}(-h_j). \tag{A7}$$

Here, $\boldsymbol{H}_{\rm s}(-h_j)$ means that all other parameters h_l with $l \neq j$ keep unchanged. For the special case with $h_4 = 0$, one has $\gamma_4 \boldsymbol{H}_{\rm s} \gamma_4 = -\boldsymbol{H}_{\rm s}$, which guarantees that if there is an eigenvalue E, then there must be an eigenvalue $-E$.

A second symmetry is similar to the time reversal symmetry given by $\mathcal{T} = \gamma_2\gamma_4\boldsymbol{K}$ with $\boldsymbol{K}$ being the complex conjugate operator that forms the complex conjugate of any coefficient that multiplies a ket. One can check that

$$\mathcal{T}\boldsymbol{H}_{\rm s}\mathcal{T}^{-1} = \boldsymbol{H}_{\rm s}. \tag{A8}$$

This symmetry guarantees that each eigenvalue is always doubly degenerate, i.e., Kramers degeneracy.

A third point is that the Hamiltonian $\boldsymbol{H}_{\rm s}$ can be block diagonalized by a unitary transformation. Let us define

$$\boldsymbol{U}_1 = \frac{1}{h}\begin{pmatrix} \boldsymbol{h'}\cdot\boldsymbol{\sigma} - {\rm i}h_2 & 0 \\ 0 & h \end{pmatrix}, \tag{A9}$$

with $\boldsymbol{h'} = (h_1, h_3, h_4)$ and $h = \sqrt{h_1^2 + h_2^2 + h_3^2 + h_4^2}$, and

$$\boldsymbol{U}_2 = \begin{pmatrix} 1 & 0 & 0 & 0 \\ 0 & 0 & 1 & 0 \\ 0 & 1 & 0 & 0 \\ 0 & 0 & 0 & 1 \end{pmatrix}. \tag{A10}$$

We then have a block-diagonalized matrix

$$\boldsymbol{U}_2^\dagger \boldsymbol{U}_1^\dagger \boldsymbol{H}_{\rm s} \boldsymbol{U}_1 \boldsymbol{U}_2 = \begin{pmatrix} h_0 & h & 0 & 0 \\ h & -h_0 & 0 & 0 \\ 0 & 0 & h_0 & h \\ 0 & 0 & h & -h_0 \end{pmatrix}. \tag{A11}$$

Acknowledgements

Project supported by the National Key Research and Development Program of China (Grant No. 2021YFA1200700), the National Natural Science Foundation of China (Grant Nos. 11905054, 12275075 and 12105094), and the Fundamental Research Funds for the Central Universities of China.

References

[1] Klitzing K V, Dorda G and Pepper M 1980 *Phys. Rev. Lett.* **45** 494
[2] Laughlin R B 1981 *Phys. Rev. B* **23** 5632
[3] Halperin B I 1982 *Phys. Rev. B* **25** 2185
[4] Haldane F D M 1988 *Phys. Rev. Lett.* **61** 2015
[5] Bernevig B A, Hughes T L and Zhang S C 2006 *Science* **314** 1757
[6] Haldane F D M and Raghu S 2008 *Phys. Rev. Lett.* **100** 013904
[7] Khanikaev A B, Mousavi S H, Tse W K, Kargarian M, MacDonald A H and Shvets G 2013 *Nat. Mater.* **12** 233
[8] Thouless D J, Kohmoto M, Nightingale M P and den Nijs M 1982 *Phys. Rev. Lett.* **49** 405
[9] Hasan M Z and Kane C L 2010 *Rev. Mod. Phys.* **82** 3045
[10] Qi X L and Zhang S C 2011 *Rev. Mod. Phys.* **83** 1057
[11] Aidelsburger M, Atala M, Lohse M, Barreiro J T, Paredes B and Bloch I 2013 *Phys. Rev. Lett.* **111** 185301
[12] Miyake H, Siviloglou G A, Kennedy C J, Burton W C and Ketterle W 2013 *Phys. Rev. Lett.* **111** 185302
[13] Aidelsburger M, Lohse M, Schweizer C, Atala M, Barreiro J T, Nascimbne S, Cooper N R, Bloch I and Goldman N 2015 *Nat. Phys.* **11** 162
[14] Eisert J, Friesdorf M and Gogolin C 2015 *Nat. Phys.* **11** 124
[15] Wang Z Y, Cheng X C, Wang B Z, Zhang J Y, Lu Y H, Yi C R, Niu S, Deng Y J, Liu X J, Chen S and Pan J W 2021 *Science* **372** 271
[16] McGinley M and Cooper N R 2019 *Phys. Rev. B* **99** 075148
[17] Heyl M, Polkovnikov A and Kehrein S 2013 *Phys. Rev. Lett.* **110** 135704
[18] Heyl M 2014 *Phys. Rev. Lett.* **113** 205701
[19] Zunkovic B, Heyl M, Knap M and Silva A 2018 *Phys. Rev. Lett.* **120** 130601
[20] Corps A L and Relano A 2023 *Phys. Rev. Lett.* **130** 100402
[21] Pastori L, Barbarino S and Budich J C 2020 *Phys. Rev. Res.* **2** 033259
[22] Lee T E, Reiter F and Moiseyev N 2014 *Phys. Rev. Lett.* **113** 250401
[23] Zhu B, Ke Y G, Zhong H H and Lee C H 2020 *Phys. Rev. Res.* **2** 023043
[24] Zhang L, Zhang L, Niu S and Liu X J 2018 *Sci. Bull.* **63** 1385
[25] Sun W, Yi C R, Wang B Z, Zhang W W, Sanders B C, Xu X T, Wang Z Y, Schmiedmayer J, Deng Y J, Liu X J, Chen S and Pan J W 2018 *Phys. Rev. Lett.* **121** 250403
[26] Yi C R, Zhang L, Zhang L, Jiao R H, Cheng X C, Wang Z Y, Xu X T, Sun W, Liu X J, Chen S and Pan J W 2019 *Phys. Rev. Lett.* **123** 190603
[27] Wang Y, Ji W T, Chai Z H, Guo Y H, Wang M Q, Ye X Y, Yu P, Zhang L, Qin X, Wang P F, Shi F Z, Rong X, Lu D W, Liu X J and Du J F 2019 *Phys. Rev. A* **100** 052328
[28] Liu X J, Liu Z X and Cheng M 2013 *Phys. Rev. Lett.* **110** 076401
[29] Liu X J, Law K T and Ng T K 2014 *Phys. Rev. Lett.* **112** 086401
[30] Bayat A, Alkurtass B, Sodano P, Johannesson H and Bose S 2018 *Phys. Rev. Lett.* **121** 030601
[31] Zhang L, Zhang L, Hu Y, Niu S and Liu X J 2021 *Phys. Rev. B* **103** 224308
[32] Ye J C and Li F X 2020 *Phys. Rev. A* **102** 042209
[33] Fang P, Wang Y X and Li F 2022 *Phys. Rev. A* **106** 022219
[34] Landau L D and Lifshitz E M 1980 *Quantum Mechanics* (Oxford: Butterworth-Heinemann)
[35] Sinitsyn N A 2014 *Phys. Rev. A* **90** 062509
[36] Sinitsyn N A, Yuzbashyan E A, Chernyak V Y, Patra A and Sun C 2018 *Phys. Rev. Lett.* **120** 190402
[37] Sinitsyn N A and Li F 2016 *Phys. Rev. A* **93** 063859
[38] Zhang L, Jia W and Liu X J 2022 *Sci. Bull.* **67** 1236
[39] Yu L X, Ji T W, Zhang L, Wang Y, Wu J S and Liu X J 2021 *Phys. Rev. X Quantum* **2** 020320
[40] Li F, Sun C, Chernyak V Y and Sinitsyn N A 2017 *Phys. Rev. A* **96** 022107
[41] del Campo A, Kibble T W and Zurek W H 2013 *J. Phys. Condens. Matter* **25** 404210
[42] Farhi E, Goldstone J, Gutmann S, Lapan J, Ludgren A and Preda D 2001 *Science* **292** 472
[43] Demkov Y N and Ostrovsky V N 2001 *J. Phys. B* **34** 2419
[44] Sinitsyn N A and Li F 2016 *Phys. Rev. A* **93** 063859
[45] Schnyder A P, Ryu S, Furusaki A and Ludwig A W W 2008 *Phys. Rev. B* **78** 195125
[46] Sinitsyn N A, Lin J and Chernyak V Y 2017 *Phys. Rev. A* **95** 012140
[47] Sinitsyn N A 2014 *Phys. Rev. A* **90** 062509
[48] Fu L and Kane C L 2006 *Phys. Rev. B* **74** 195312
[49] Fu L and Kane C L 2007 *Phys. Rev. B* **76** 045302
[50] Rachel S and Le H K 2010 *Phys. Rev. B* **82** 075106
[51] Hohenadler M, Lang T C and Assaad F F 2011 *Phys. Rev. Lett.* **106** 100403